Quaternary phases with Fe$_2$P-type structure in *R*–Ag–Al–Ge systems (*R* = Pr, Sm)

Roksolana KOZAK[1]*, Oksana ZAHARKO[2], Antonio CERVELLINO[3], Lev AKSELRUD[1], Roman GLADYSHEVSKII[1]

[1] *Department of Inorganic Chemistry, Ivan Franko National University of Lviv,*
   Kyryla i Mefodiya St. 6, 79005 Lviv, Ukraine
[2] *Laboratory for Neutron Scattering, ETHZ & PSI, CH-5232 Villigen, Switzerland*
[3] *Swiss Light Source, Paul Scherrer Institute, CH-5232 Villigen, Switzerland*
* Corresponding author. E-mail: r-kozak@ukr.net

The existence of limited solid solutions based on the ternary compounds PrAg$_{1.40-1.20}$Ge$_{0.60-0.80}$ and SmAg$_{1.40-0.98}$Ge$_{0.60-1.02}$ with Fe$_2$P-type structure (*hP*9, *P*6̄2*m*), was established at 33.3 at.% *R* in the quaternary systems *R*–Ag–Al–Ge (*R* = Pr, Sm) at 873 K. The crystal structures of the solid solutions were determined from conventional X-ray (*a* = 0.7232(1), *c* = 0.44081(8) nm for the composition PrAg$_{0.90}$Al$_{0.35}$Ge$_{0.75}$ and *a* = 0.71180(5), *c* = 0.43634(5) nm for SmAg$_{0.90}$Al$_{0.39}$Ge$_{0.71}$) and synchrotron (*a* = 0.72311(2), *c* = 0.44101(2) nm for PrAg$_{0.87}$Al$_{0.38}$Ge$_{0.75}$) powder diffraction data. A statistical mixture of Ag and Al atoms occupy the 3*g* site and forms columns of trigonal prisms with Ge atoms at the center (1*a* site), whereas a statistical mixture of Ge and Ag atoms is situated at the centers of the trigonal prisms *R*$_6$ (2*d* site).

Rare-earth / Silver / Aluminum / Germanium / Solid solution / X-ray diffraction / Crystal structure

Introduction

The existence of ternary compounds with the hexagonal Fe$_2$P-type structure (Pearson symbol *hP*9, space group *P*6̄2*m*) in the *R*Ag$_2$–*R*Ge$_2$ cross-section of the *R*–Ag–Ge systems, where *R* is a rare-earth element or Y, has previously been reported [1-3]. These compounds are formed with La, Ce, Pr, Nd and Sm (873 K) and their compositions have been reported as *R*Ag$_{1.4}$Ge$_{0.6}$, except for NdAg$_{1.1}$Ge$_{0.9}$. The structure is characterized by trigonal-prismatic coordination of the small atoms. The *R* and, mainly, Ag atoms build trigonal prisms, while a statistical mixture Ag+Ge (with predominantly Ge atoms) occupies the centres of the prisms [1]. The equiatomic compounds *R*AgGe formed with Sm, Gd and rare-earth elements of the yttrium subgroup (973 K) belong to the ZrNiAl structure type, a ternary variant of the Fe$_2$P type [4]. In these ordered structures the Ge atoms are located at the centers of *R*$_6$ and Ag$_6$ trigonal prisms. In rare-earth alumogermanides containing transition metals, the trigonal prisms are built by *R* and Al atoms, while the *d*-element atoms are situated at the prism centers [5,6]. In the structure type Y$_3$NiAl$_3$Ge$_2$ [5], a quaternary substitution variant of Fe$_2$P, the centers of the larger trigonal prisms (Y$_6$) are occupied by Ge atoms, while the Ni atoms are in the smaller prisms (Al$_6$). The distribution of atoms at the different Wyckoff positions in compounds with the Fe$_2$P, ZrNiAl and Y$_3$NiAl$_3$Ge$_2$ structure types is shown in Table 1.

In this work we present data on the homogeneity range and crystal structure of the solid solutions based on the ternary compounds PrAg$_{1.4}$Ge$_{0.6}$ and SmAg$_{1.4}$Ge$_{0.6}$ with Fe$_2$P-type structure, in the *R*Ag$_2$–*R*Al$_2$–*R*Ge$_2$ cross-section of the quaternary systems *R*–Ag–Al–Ge (*R* = Pr, Sm) at 873 K.

Experimental

The alloys (6 three-component and 20 four-component), each with a total weight of 1 g, were synthesized by arc melting of the constituent elements (with purities Pr, Sm ≥ 99.83%, Al ≥ 99.985%, Ag ≥ 99.99% and Ge ≥ 99.999%) in a water-cooled copper crucible under a purified argon atmosphere, using Ti as a getter and a tungsten electrode. For homogenization the samples were vacuum-sealed in quartz ampoules, annealed at 873 K for 720 h and subsequently quenched into cold water. Phase analysis, determination of the unit-cell parameters and refinement of the crystal structures were made based on X-ray powder diffraction data collected on a diffractometer DRON-2.0M (Fe *K*α radiation) in the angular range 20 ≤ 2*θ* ≤ 100º with the step 0.05º. In addition, high-resolution X-ray synchrotron

Table 1 Atom distribution over the Wyckoff positions in some rare-earth germanides and aluminides with the Fe$_2$P, ZrNiAl and Y$_3$NiAl$_3$Ge$_2$ structure types.

Structure type	Wyckoff position			
	3f	**3g**	**2d**	**1a**
Fe$_2$P		Ag >> Ge	Ag < Ge	Ag < Ge
ZrNiAl	*R*	Ag	Ge	Ge
		Al	Ni	Ni
Y$_3$NiAl$_3$Ge$_2$		Al	Ge	Ni

Table 2 Phases detected in alloys of the Pr–Ag–Al–Ge system at 873 K.

No.	Sample composition, at.%	Phase [a]	Structure type	Unit-cell parameters			
				a, nm	*b*, nm	*c*, nm	*V*, nm^3
1	Pr$_{33.3}$Ag$_{46.7}$Ge$_{20.0}$	**Pr$_{14}$Ag$_{51}$**	Gd$_{14}$Ag$_{51}$	1.2849(6)	–	0.9458(5)	1.352(1)
		PrAg$_{1.40-1.20}$Ge$_{0.60-0.80}$	Fe$_2$P	0.7379(3)	–	0.4306(2)	0.2030(2)
		PrAg$_2$	KHg$_2$	0.4849(4)	0.6967(5)	0.8146(1)	0.2752(5)
2	Pr$_{33.3}$Ag$_{43.4}$Ge$_{23.3}$	**PrAg$_{1.40-1.20}$Ge$_{0.60-0.80}$**	Fe$_2$P	0.7306(2)	–	0.4326(1)	0.2000(1)
		Pr$_{14}$Ag$_{51}$	Gd$_{14}$Ag$_{51}$	1.2825(5)	–	0.9441(5)	1.345(1)
		PrAg$_2$	KHg$_2$	0.4821(8)	0.6917(9)	0.8250(4)	0.2751(6)
3	Pr$_{33.3}$Ag$_{40.0}$Ge$_{26.7}$	**PrAg$_{1.40-1.20}$Ge$_{0.60-0.80}$**	Fe$_2$P	0.7302(1)	–	0.43319(8)	0.20002(6)
		Pr$_{14}$Ag$_{51}$	Gd$_{14}$Ag$_{51}$	1.2836(4)	–	0.9434(4)	1.3461(8)
4	Pr$_{33.3}$Ag$_{40.0}$Al$_{3.3}$Ge$_{23.4}$	**I**	Fe$_2$P	0.7306(2)	–	0.4333(1)	0.20027(9)
5	Pr$_{33.3}$Ag$_{40.0}$Al$_{6.7}$Ge$_{20.0}$	**I**	Fe$_2$P	0.73162(9)	–	0.43352(7)	0.20096(5)
6	Pr$_{33.3}$Ag$_{40.0}$Al$_{10.0}$Ge$_{16.7}$	**I**	Fe$_2$P	0.7300(2)	–	0.4348(1)	0.20067(9)
7	Pr$_{33.3}$Ag$_{33.4}$Al$_{3.3}$Ge$_{30.0}$	**I**	Fe$_2$P	0.72987(9)	–	0.43341(6)	0.19995(5)
8	Pr$_{33.3}$Ag$_{33.3}$Al$_{8.4}$Ge$_{25.0}$	**I**	Fe$_2$P	0.7286(1)	–	0.4350(1)	0.20000(7)
9	Pr$_{33.3}$Ag$_{33.3}$Al$_{11.1}$Ge$_{22.3}$	**I**	Fe$_2$P	0.7286(1)	–	0.43596(8)	0.20045(6)
10	Pr$_{33.3}$Ag$_{33.4}$Al$_{13.3}$Ge$_{20.0}$	**I**	Fe$_2$P	0.72771(9)	–	0.43689(7)	0.20036(5)
11	Pr$_{33.3}$Ag$_{33.3}$Al$_{16.7}$Ge$_{16.7}$	**I**	Fe$_2$P	0.7253(2)	–	0.4391(2)	0.2001(1)
12	Pr$_{33.3}$Ag$_{30.0}$Al$_{6.7}$Ge$_{30.0}$	**I**	Fe$_2$P	0.72842(9)	–	0.43426(7)	0.19952(5)
13	Pr$_{33.3}$Ag$_{26.7}$Al$_{16.0}$Ge$_{24.0}$	**I**	Fe$_2$P	0.7247(1)	–	0.4389(1)	0.19961(7)
14	Pr$_{33.3}$Ag$_{26.7}$Al$_{20.0}$Ge$_{20.0}$	**I**	Fe$_2$P	0.7232(1)	–	0.44081(8)	0.19966(5)
15	Pr$_{33.3}$Ag$_{22.2}$Al$_{22.2}$Ge$_{22.3}$	**I**	Fe$_2$P	0.7234(1)	–	0.44097(9)	0.19984(7)
		PrAl$_{1.42-0.98}$Ge$_{0.58-1.02}$	α-ThSi$_2$	0.4279(1)	–	1.4824(7)	0.2714(2)

[a] I – quaternary phase based on ternary compound PrAg$_{1.40-1.20}$Ge$_{0.60-0.80}$.

diffraction data for the sample Pr$_{33.3}$Ag$_{26.7}$Al$_{20.0}$Ge$_{20.0}$ were collected on the Materials Science beamline at the Swiss Light Source. The wavelength of the synchrotron radiation (λ = 0.049063 nm) was determined by refining the silicon pattern (a = 0.54310204 nm). The profile and structural parameters were refined by the Rietveld method using the DBWS-9807 [7] and WinCSD [8] program packages.

Results and discussion

The phases detected in the different samples and refined unit-cell parameters for the compounds identified at 873 K in the Pr–Ag–Al–Ge and Sm–Ag–Al–Ge systems are shown in Table 2 and Table 3, respectively. Based on X-ray powder diffraction data, the existence of the compounds PrAg$_{1.4}$Ge$_{0.6}$ (structure type Fe$_2$P, space group *P*$\bar{6}$2*m*), PrAl$_{1.42-0.98}$Ge$_{0.58-1.02}$ (α-ThSi$_2$, *I*4$_1$/*amd*), Pr$_{14}$Ag$_{51}$ (Gd$_{14}$Ag$_{51}$, *P*6/*m*) and

SmAg$_{1.4}$Ge$_{0.6}$ (Fe$_2$P, *P*$\bar{6}$2*m*), Sm$_3$Ag$_4$Ge$_4$ (Gd$_3$Cu$_4$Ge$_4$, *Immm*), and Sm$_{14}$Ag$_{51}$ (Gd$_{14}$Ag$_{51}$, *P*6/*m*) was confirmed.

For the compounds PrAg$_{1.4}$Ge$_{0.6}$ and SmAg$_{1.4}$Ge$_{0.6}$ the existence of homogeneity ranges in the ternary systems has been established and their compositions can be presented as PrAg$_{1.40-1.20}$Ge$_{0.60-0.80}$ and SmAg$_{1.40-0.98}$Ge$_{0.60-1.02}$. The variation of the unit-cell parameters for PrAg$_{1.40-1.20}$Ge$_{0.60-0.80}$ and SmAg$_{1.40-0.98}$Ge$_{0.60-1.02}$ as a function of the Ge content is shown in Fig. 1 and Fig. 2, respectively. Within the homogeneity range of the ternary compounds (33.3 at.% *R*) the *c*-parameter increases with decreasing Ag (46.7-32.7 at.%) and increasing Ge (20.0-34.0 at.%) content, whereas the *a*-parameter and unit-cell volume *V* decrease when Ag atoms (atomic radius *r* = 0.144 nm) are replaced by Ge atoms (r = 0.137 nm).

All the four-component alloys, except Pr$_{33.3}$Ag$_{22.2}$Al$_{22.2}$Ge$_{22.3}$ and Sm$_{33.3}$Ag$_{26.7}$Al$_{13.3}$Ge$_{26.7}$, were single-phase samples. Consequently, limited

Table 3 Phases detected in alloys of the Sm–Ag–Al–Ge system at 873 K.

No.	Sample composition, at.%	Phase [a]	Structure type	Unit-cell parameters			
				a, nm	*b*, nm	*c*, nm	*V*, nm³
1	$Sm_{33.3}Ag_{46.7}Ge_{20.0}$	**$SmAg_{1.40-0.98}Ge_{0.60-1.02}$**	Fe_2P	0.7237(2)	–	0.4249(1)	0.19274(9)
		$Sm_{14}Ag_{51}$	$Gd_{14}Ag_{51}$	1.2724(4)	–	0.9361(4)	1.3124(8)
		X	...	...	...	...	...
2	$Sm_{33.3}Ag_{43.4}Ge_{23.3}$	**$SmAg_{1.40-0.98}Ge_{0.60-1.02}$**	Fe_2P	0.7227(1)	–	0.42585(9)	0.19261(6)
		$Sm_{14}Ag_{51}$	$Gd_{14}Ag_{51}$	1.2727(4)	–	0.9359(5)	1.3129(9)
3	$Sm_{33.3}Ag_{40.0}Ge_{26.7}$	**$SmAg_{1.40-0.98}Ge_{0.60-1.02}$**	Fe_2P	0.72195(8)	–	0.42623(6)	0.19239(4)
		$Sm_{14}Ag_{51}$	$Gd_{14}Ag_{51}$	1.2736(5)	–	0.9363(8)	1.315(1)
4	$Sm_{33.3}Ag_{33.3}Ge_{33.4}$	**$SmAg_{1.40-0.98}Ge_{0.60-1.02}$**	Fe_2P	0.72059(5)	–	0.42672(4)	0.19189(2)
		$Sm_3Ag_4Ge_4$	$Gd_3Cu_4Ge_4$	0.4376(1)	0.7086(2)	1.4565(3)	0.4517(2)
5	$Sm_{33.3}Ag_{26.7}Ge_{40.0}$	**$Sm_3Ag_4Ge_4$**	$Gd_3Cu_4Ge_4$	0.43728(5)	0.70924(7)	1.4566(2)	0.45174(8)
		$SmAg_{1.40-0.98}Ge_{0.60-1.02}$	Fe_2P	0.72022(9)	–	0.42688(9)	0.19176(5)
		$SmGe_{2-x}$	α-$ThSi_2$	0.41344(9)	–	1.3896(4)	0.2375(1)
6	$Sm_{33.3}Ag_{33.4}Al_{6.7}Ge_{26.6}$	**II**	Fe_2P	0.71898(6)	–	0.42860(4)	0.19188(3)
7	$Sm_{33.3}Ag_{33.4}Al_{10.0}Ge_{23.3}$	**II**	Fe_2P	0.71870(6)	–	0.42969(4)	0.19221(3)
8	$Sm_{33.3}Ag_{33.4}Al_{13.3}Ge_{20.0}$	**II**	Fe_2P	0.7185(1)	–	0.43035(8)	0.19239(5)
9	$Sm_{33.3}Ag_{30.0}Al_{6.7}Ge_{30.0}$	**II**	Fe_2P	0.7176(1)	–	0.42995(7)	0.19174(5)
10	$Sm_{33.3}Ag_{26.7}Al_{13.3}Ge_{26.7}$	**II**	Fe_2P	0.7147(1)	–	0.43313(9)	0.19158(6)
		$Sm_3Ag_4Ge_4$	$Gd_3Cu_4Ge_4$	0.4435(4)	0.6965(8)	1.461(1)	0.4517(8)
11	$Sm_{33.3}Ag_{26.7}Al_{16.7}Ge_{23.3}$	**II**	Fe_2P	0.71276(6)	–	0.43503(5)	0.19140(3)
12	$Sm_{33.3}Ag_{26.7}Al_{20.0}Ge_{20.0}$	**II**	Fe_2P	0.71180(5)	–	0.43634(5)	0.19146(3)
13	$Sm_{33.3}Ag_{22.2}Al_{22.2}Ge_{22.3}$	**II**	Fe_2P	0.71107(7)	–	0.43604(6)	0.19093(4)

[a] II – quaternary phase based on ternary compound $SmAg_{1.40-0.98}Ge_{0.60-1.02}$, X – unidentified phase.
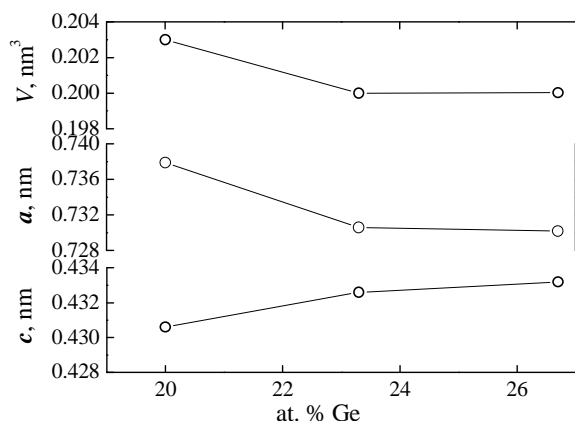

Fig. 1 Unit-cell parameters within the homogeneity range of $PrAg_{1.40-1.20}Ge_{0.60-0.80}$.

solid solutions based on the ternary compounds $PrAg_{1.40-1.20}Ge_{0.60-0.80}$ and $SmAg_{1.40-0.98}Ge_{0.60-1.02}$ with Fe_2P-type structures exist in the quaternary systems {Pr,Sm}–Ag–Al–Ge at 33.3 at.% *R* and 873 K [9-11]. For these homogeneity ranges the *a*-parameter decreases with increasing Al (0-22.2 at.%) and decreasing Ge (33.4-16.7 at.%) or Ag (46.7-22.2 at.%) content for a fixed Ag or Ge content, whereas the *c*-parameter increases (Figs. 3-6). The contact distances between the small atoms in the Fe_2P-type structure are mainly situated in the *ab* plane. The change of the unit-cell parameters within the solid solutions is in agreement with the atomic radii of the

elements (r_{Ag} = 0.144, r_{Al} = 0.143, r_{Ge} = 0.137 nm). It may be noticed that the average radius of the small-size atoms ($r_M = (xr_{Ag}+yr_{Al}+zr_{Ge})/(x+y+z)$, where x, y and z are the relative quantities of Ag, Al and Ge in the statistical mixture M = Ag+Al+Ge) for the limiting compositions is almost the same (Tables 4,5). In addition to the atom-size factor, the replacement of Ge atoms with four valence electrons (or Ag atoms with one valence electron) by Al atoms with three valence electrons increases (or decreases) the valence electron concentration per atom of the statistical mixture M (VEC_A [12]). For the solids solutions based on the ternary compounds with Fe_2P-type structure,
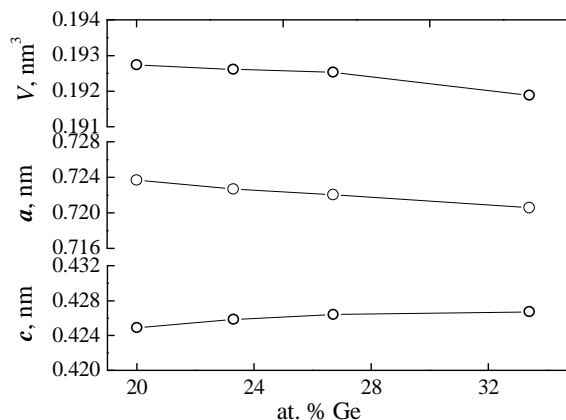

Fig. 2 Unit-cell parameters within the homogeneity range of $SmAg_{1.40-0.98}Ge_{0.60-1.02}$.

Table 4 VEC$_A$ and height/base ratio of the trigonal prisms Pr$_6$ and M_6 for the solid solution based on PrAg$_{1.40-1.20}$Ge$_{0.60-0.80}$, Fe$_2$P structure type.

Sample composition, at.%	VEC$_A$	r_M, nm	x_{Pr}	x_{M3}	Height of Pr$_6$	Height/base ratio of Pr$_6$	Height of M_6	Height/base ratio of M_6
Pr$_{33.3}$Ag$_{40.0}$Ge$_{26.7}$	3.70	0.1413	0.585(2)	0.245(2)	0.3806	1.1382	0.3099	1.3980
Pr$_{33.3}$Ag$_{40.0}$Al$_{3.3}$Ge$_{23.4}$	3.65	0.1415	0.589(1)	0.232(2)	0.3823	1.1335	0.2936	1.4759
Pr$_{33.3}$Ag$_{40.0}$Al$_{6.7}$Ge$_{20.0}$	3.60	0.1418	0.575(1)	0.238(2)	0.3779	1.1471	0.3016	1.4375
Pr$_{33.3}$Ag$_{40.0}$Al$_{10.0}$Ge$_{16.7}$	3.55	0.1421	0.579(2)	0.237(3)	0.3784	1.1490	0.2997	1.4510
Pr$_{33.3}$Ag$_{33.4}$Al$_{3.3}$Ge$_{30.0}$	3.95	0.1408	0.585(1)	0.247(2)	0.3804	1.1392	0.3123	1.3880
Pr$_{33.3}$Ag$_{33.3}$Al$_{8.4}$Ge$_{25.0}$	3.88	0.1413	0.577(1)	0.246(2)	0.3770	1.1537	0.3105	1.4012
Pr$_{33.3}$Ag$_{33.3}$Al$_{11.1}$Ge$_{22.3}$	3.84	0.1415	0.576(2)	0.245(2)	0.3767	1.1573	0.3092	1.4100
Pr$_{33.3}$Ag$_{33.4}$Al$_{13.3}$Ge$_{20.0}$	3.80	0.1418	0.577(1)	0.241(2)	0.3766	1.1602	0.3038	1.4383
Pr$_{33.3}$Ag$_{33.3}$Al$_{16.7}$Ge$_{16.7}$	3.75	0.1420	0.573(3)	0.247(2)	0.3741	1.1739	0.3103	1.4151
Pr$_{33.3}$Ag$_{30.0}$Al$_{6.7}$Ge$_{30.0}$	4.05	0.1408	0.589(1)	0.243(2)	0.3811	1.1394	0.3066	1.4165
Pr$_{33.3}$Ag$_{26.7}$Al$_{16.0}$Ge$_{24.0}$	4.06	0.1412	0.577(2)	0.241(2)	0.3750	1.1703	0.3025	1.4509
Pr$_{33.3}$Ag$_{26.7}$Al$_{20.0}$Ge$_{20.0}$	4.00	0.1417	0.577(1)	0.242(2)	0.3742	1.1777	0.3031	1.4540
Pr$_{33.3}$Ag$_{22.2}$Al$_{22.2}$Ge$_{22.3}$	4.16	0.1414	0.576(2)	0.245(3)	0.3740	1.1790	0.3070	1.4365

Table 5 VEC$_A$ and height/base ratio of the trigonal prisms Sm$_6$ and M_6 for the solid solution based on SmAg$_{1.40-0.98}$Ge$_{0.60-1.02}$, Fe$_2$P structure type.

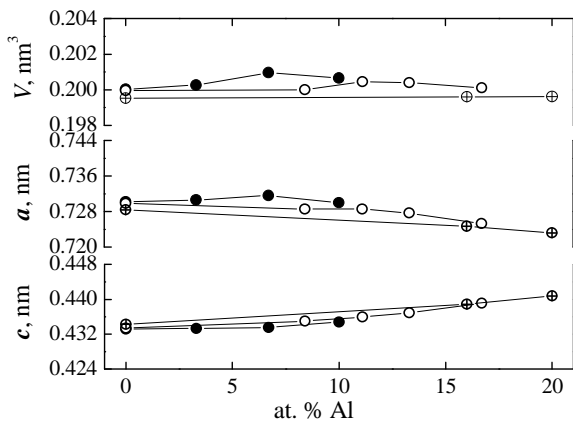| Sample composition, at.%	VEC$_A$	r_M, nm	x_{Sm}	x_{M3}	Height of Sm$_6$	Height/base ratio of Sm$_6$	Height of M_6	Height/base ratio of M_6
Sm$_{33.3}$Ag$_{40.0}$Ge$_{26.7}$	3.70	0.1413	0.584(1)	0.245(1)	0.3760	1.1340	0.3064	1.3915
Sm$_{33.3}$Ag$_{33.3}$Ge$_{33.4}$	4.00	0.1406	0.5848(8)	0.243(1)	0.3756	1.1361	0.3033	1.4069
Sm$_{33.3}$Ag$_{33.4}$Al$_{6.7}$Ge$_{26.6}$	3.90	0.1412	0.5769(9)	0.245(1)	0.3721	1.1519	0.3051	1.4047
Sm$_{33.3}$Ag$_{33.4}$Al$_{10.0}$Ge$_{23.3}$	3.85	0.1415	0.5776(8)	0.242(1)	0.3722	1.1544	0.3012	1.4264
Sm$_{33.3}$Ag$_{33.4}$Al$_{13.3}$Ge$_{20.0}$	3.80	0.1418	0.576(1)	0.240(1)	0.3715	1.1586	0.2987	1.4410
Sm$_{33.3}$Ag$_{30.0}$Al$_{6.7}$Ge$_{30.0}$	4.05	0.1408	0.586(1)	0.236(2)	0.3744	1.1483	0.2946	1.4594
Sm$_{33.3}$Ag$_{26.7}$Al$_{13.3}$Ge$_{26.7}$	4.10	0.1411	0.579(1)	0.235(2)	0.3705	1.1690	0.2909	1.4888
Sm$_{33.3}$Ag$_{26.7}$Al$_{16.7}$Ge$_{23.3}$	4.05	0.1414	0.5780(8)	0.245(2)	0.3692	1.1783	0.3025	1.4381
Sm$_{33.3}$Ag$_{26.7}$Al$_{20.0}$Ge$_{20.0}$	4.00	0.1417	0.5743(8)	0.240(2)	0.3674	1.1875	0.2959	1.4745
Sm$_{33.3}$Ag$_{22.2}$Al$_{22.2}$Ge$_{22.3}$	4.16	0.1414	0.579(1)	0.245(2)	0.3686	1.1828	0.3018	1.4449

Fig. 3 Unit-cell parameters for the solid solution based on PrAg$_{1.40-1.20}$Ge$_{0.60-0.80}$ along the lines 26.7 (⊕), 33.3 (○) and 40.0 (●) at.% Ag.
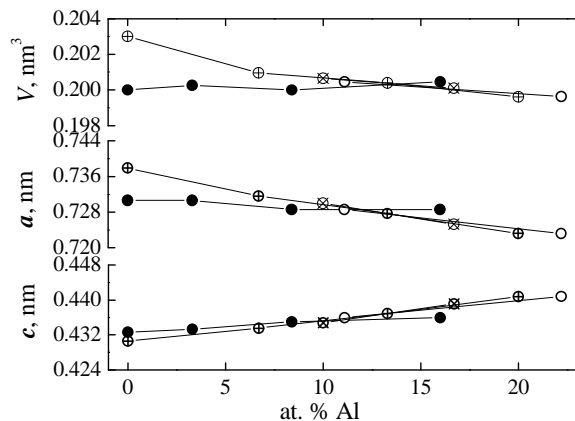

Fig. 4 Unit-cell parameters for the solid solution based on PrAg$_{1.40-1.20}$Ge$_{0.60-0.80}$ along the lines 16.7 (⊗), 20.0 (⊕), 22.2 (○) and 23.3-25.0 (●) at.% Ge.

PrAg$_{1.40-1.20}$Ge$_{0.60-0.80}$ and SmAg$_{1.40-0.98}$Ge$_{0.60-1.02}$, VEC$_A$ is in the range 3.55-4.17. In comparison, for the other solid solutions observed in the systems {Pr,Sm}–Ag–Al–Ge at 33.3 at.% *R* and 873 K, VEC$_A$ = 4.77-5.00 (α-ThSi$_2$-type structure) and 4.30-4.76 (AlB$_2$-type structure).

Table 6 Ag/Al and Ge/Ag ratios of different Wyckoff positions for alloys belonging to the Fe$_2$P-type solid solution in the Pr–Ag–Al–Ge system (from conventional XRD).

Sample composition, at.%	Ag/Al 3*g*	Ge/Ag 2*d*	Ge/Ag 1*a*
Pr$_{33.3}$Ag$_{40.0}$Ge$_{26.7}$	100/0	99/1	64/36
Pr$_{33.3}$Ag$_{40.0}$Al$_{3.3}$Ge$_{23.4}$	93/8	80/20	63/37
Pr$_{33.3}$Ag$_{40.0}$Al$_{6.7}$Ge$_{20.0}$	100/0	68/32	62/38
Pr$_{33.3}$Ag$_{40.0}$Al$_{10.0}$Ge$_{16.7}$	78/22	68/32	100/0
Pr$_{33.3}$Ag$_{33.4}$Al$_{3.3}$Ge$_{30.0}$	100/0	71/29	97/3
Pr$_{33.3}$Ag$_{33.3}$Al$_{8.4}$Ge$_{25.0}$	100/0	87/13	97/3
Pr$_{33.3}$Ag$_{33.3}$Al$_{11.1}$Ge$_{22.3}$	88/12	56/44	99/1
Pr$_{33.3}$Ag$_{33.4}$Al$_{13.3}$Ge$_{20.0}$	80/20	60/40	94/6
Pr$_{33.3}$Ag$_{33.3}$Al$_{16.7}$Ge$_{16.7}$	63/37	36/64	94/6
Pr$_{33.3}$Ag$_{30.0}$Al$_{6.7}$Ge$_{30.0}$	84/16	96/4	95/5
Pr$_{33.3}$Ag$_{26.7}$Al$_{16.0}$Ge$_{24.0}$	77/23	72/28	95/5
Pr$_{33.3}$Ag$_{26.7}$Al$_{20.0}$Ge$_{20.0}$	66/34	78/22	68/32
Pr$_{33.3}$Ag$_{22.2}$Al$_{22.2}$Ge$_{22.3}$	62/38	80/20	91/9

Table 7 Ag/Al and Ge/Ag ratios of different Wyckoff positions for alloys belonging to the Fe$_2$P-type solid solution in the Sm–Ag–Al–Ge system (from conventional XRD).

Sample composition, at.%	Ag/Al 3*g*	Ge/Ag 2*d*	Ge/Ag 1*a*
Sm$_{33.3}$Ag$_{40.0}$Ge$_{26.7}$	73/27	50/50	92/8
Sm$_{33.3}$Ag$_{33.3}$Ge$_{33.4}$	85/15	93/7	94/6
Sm$_{33.3}$Ag$_{33.4}$Al$_{6.7}$Ge$_{26.6}$	92/8	56/44	100/0
Sm$_{33.3}$Ag$_{33.4}$Al$_{10.0}$Ge$_{23.3}$	81/19	80/20	100/0
Sm$_{33.3}$Ag$_{33.4}$Al$_{13.3}$Ge$_{20.0}$	75/25	65/35	100/0
Sm$_{33.3}$Ag$_{30.0}$Al$_{6.7}$Ge$_{30.0}$	85/15	89/11	100/0
Sm$_{33.3}$Ag$_{26.7}$Al$_{13.3}$Ge$_{26.7}$	78/22	95/5	72/28
Sm$_{33.3}$Ag$_{26.7}$Al$_{16.7}$Ge$_{23.3}$	62/38	84/16	89/11
Sm$_{33.3}$Ag$_{26.7}$Al$_{20.0}$Ge$_{20.0}$	63/37	72/28	69/31
Sm$_{33.3}$Ag$_{22.2}$Al$_{22.2}$Ge$_{22.3}$	53/47	95/5	83/17

Fig. 6 Unit-cell parameters for the solid solution based on SmAg$_{1.40-0.98}$Ge$_{0.60-1.02}$ along the lines 20.0 (⊕), 22.2-23.3 (○) and 26.7 (●) at.% Ge.

Fig. 7 Coordination polyhedra of the *R* = Pr, Sm (*a*), *M*3 (*b*), *M*2 (*c*) and *M*1(*d*) atoms in the Fe$_2$P-type structure *R*$_3$*M*3$_3$*M*2$_2$*M*1.

In the Fe$_2$P-type structure the small atoms can occupy three Wyckoff positions: 3*g*, 2*d* and 1*a* (see Table 1). We assume that Al will most likely substitute for Ag on the prism-forming site (3*g*), whereas negligible amounts of Ge are expected on the same site. Consequently, we refined the Ag/Al site for the 3*g* site and the Ge/Ag ratio for the 2*d* and 1*a* sites (Tables 6,7). Within the homogeneity range of the quaternary phases with Fe$_2$P-type structure an increase of the Al content (decrease of the Ge content) for a fixed Ag content leads to a higher Al occupation of the 3*g* site and a decrease of the amount of Ge on the 2*d* site, whereas the 1*a* site remains almost fully occupied by Ge atoms. It follows that the statistical

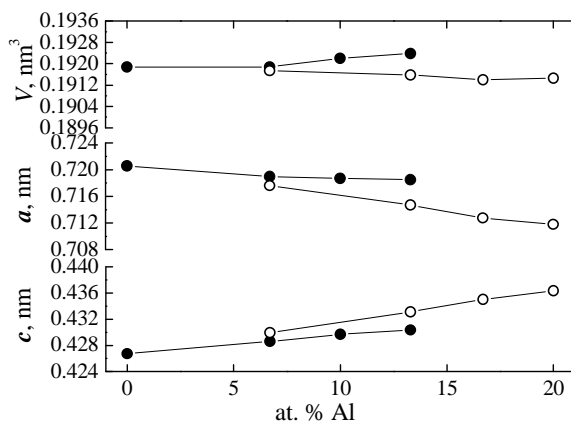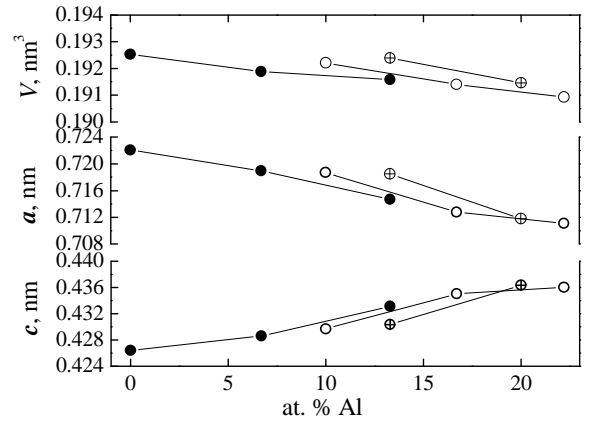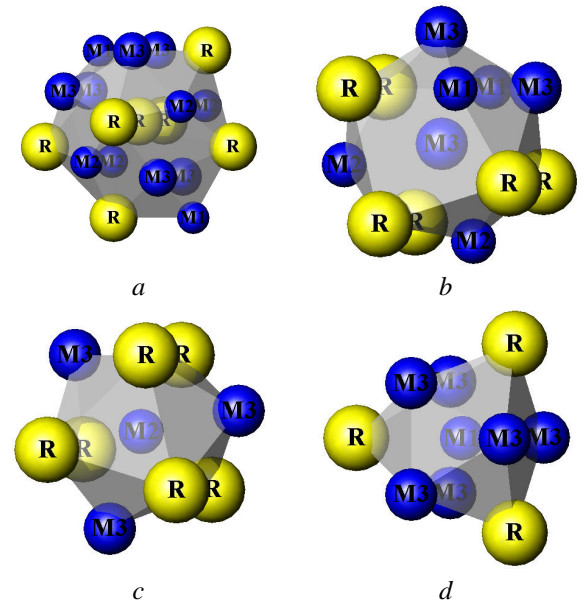**Fig. 5** Unit-cell parameters for the solid solution based on SmAg$_{1.40-0.98}$Ge$_{0.60-1.02}$ along the lines 26.7-30.0 (○) and 33.4 (●) at.% Ag.

Table 8 Details of the structure refinement for the polycrystalline samples Pr$_{33.3}$Ag$_{26.7}$Al$_{20.0}$Ge$_{20.0}$ and Sm$_{33.3}$Ag$_{26.7}$Al$_{20.0}$Ge$_{20.0}$ (Fe *K*α radiation).

Phase		PrAg$_{0.90}$Al$_{0.35}$Ge$_{0.75}$	SmAg$_{0.90}$Al$_{0.39}$Ge$_{0.71}$
Space group		*P*$\bar{6}$2*m*	*P*$\bar{6}$2*m*
Unit-cell parameters	*a*, nm	0.7232(1)	0.71180(5)
	c, nm	0.44081(8)	0.43634(5)
	V, nm^3	0.19966(5)	0.19146(3)
Formula units per cell *Z*		3	3
Density *D*$_X$, g cm^{-3}		7.549	8.055
Texture parameter *G*		0.85(1) [100]	0.801(7) [100]
FWHM parameters *U*, *V*, *W*		0.2(1), -0.01(1), 0.05(4)	0.15(4), -0.19(5), 0.12(1)
Mixing parameter *η*		0.85(4)	0.74(3)
Asymmetry parameter *C*$_M$		-0.04(3)	-0.18(2)
Number of refined parameters		16	16
Reliability factors *R*$_B$, *R*$_p$, *R*$_{wp}$		0.0930, 0.0541, 0.0681	0.0983, 0.0637, 0.0806
Goodness of fit *S*		0.85	0.73

Table 9 Atomic coordinates and isotropic displacement parameters for PrAg$_{0.90}$Al$_{0.35}$Ge$_{0.75}$ and SmAg$_{0.90}$Al$_{0.39}$Ge$_{0.71}$ (space group *P*-62*m*).

Site	Wyckoff position	*x*	*y*	*z*	*B*$_{iso}$, 10^{-2} nm^2	Occupancy
			PrAg$_{0.90}$Al$_{0.35}$Ge$_{0.75}$ *a* = 0.7232(1), *c* = 0.44081(8) nm			
Pr	3*f*	0.577(1)	0	0	0.4(3)	1
*M*3	3*g*	0.241(2)	0	1/2	0.7	0.65(3)Ag + 0.35(3)Al
*M*2	2*d*	1/3	2/3	1/2	0.7	0.22(8)Ag + 0.78(8)Ge
*M*1	1*a*	0	0	0	0.7	0.32(8)Ag + 0.68(8)Ge
			SmAg$_{0.90}$Al$_{0.39}$Ge$_{0.71}$ *a* = 0.71180(5), *c* = 0.43634(5) nm			
Sm	3*f*	0.5742(8)	0	0	0.5(2)	1
*M*3	3*g*	0.242(1)	0	1/2	0.7	0.61(5)Ag + 0.39(5)Al
*M*2	2*d*	1/3	2/3	1/2	0.7	0.26(7)Ag + 0.74(7)Ge
*M*1	1*a*	0	0	0	0.7	0.36(1)Ag + 0.64(1)Ge

mixture Ag+Al occupying the 3*g* site forms columns of trigonal prisms with almost exclusively Ge atoms at the centers (1*a* site), whereas a statistical mixture Ge+Ag is situated at the centers of the trigonal prisms *R*$_6$ on the 2*d* site.

The results of the structural refinement based on conventional X-ray diffraction data for the polycrystalline samples Pr$_{33.3}$Ag$_{26.7}$Al$_{20.0}$Ge$_{20.0}$ and Sm$_{33.3}$Ag$_{26.7}$Al$_{20.0}$Ge$_{20.0}$ are shown in Table 8. The isotropic displacement parameters of the Pr and Sm atoms were refined, while those of the Ag, Al and Ge atoms were fixed (*B*$_{iso}$ = 0.7·10^{-2} nm^2). The atomic coordinates for PrAg$_{0.90}$Al$_{0.35}$Ge$_{0.75}$ and SmAg$_{0.90}$Al$_{0.39}$Ge$_{0.71}$ are listed in Table 9, selected interatomic distances in Table 10. The Pr and Sm atoms center pseudo Frank-Kasper polyhedra with 18 apexes, which are typical for *R* atoms (Fig. 7a). The coordination polyhedra of the *M*3 atoms are distorted cubooctahedra (Fig. 7b), whereas tricapped trigonal prisms are formed around both the *M*2 (Fig. 7c) and *M*1 (Fig. 7d) atoms. Experimental details of the

structure refinement based on synchrotron diffraction data for the sample Pr$_{33.3}$Ag$_{26.7}$Al$_{20.0}$Ge$_{20.0}$ are presented in Table 11. Atomic coordinates and isotropic displacement parameters for PrAg$_{0.87}$Al$_{0.38}$Ge$_{0.75}$ are listed in Table 12, anisotropic displacement parameters in Table 13, and selected interatomic distances in Table 14. The observed, calculated and difference X-ray synchrotron diffraction patterns are shown in Fig. 8. The refined compositions (PrAg$_{0.90(2)}$Al$_{0.35(2)}$Ge$_{0.75(3)}$, SmAg$_{0.90(3)}$Al$_{0.39(3)}$Ge$_{0.71(1)}$, and PrAg$_{0.87(1)}$Al$_{0.38(1)}$Ge$_{0.75(1)}$, respectively) show a significantly lower Al content than the nominal composition of the alloy (*R*Ag$_{0.80}$Al$_{0.60}$Ge$_{0.60}$), and it cannot be excluded that part of Al substitutes on the 2*d* and 1*a* sites. It may be noted that the average number of electrons on each of the three sites occupied by small atoms is almost identical, however, crystal chemical arguments are not in favor of a statistical occupation by three elements on all these sites.

Table 10 Interatomic distances for PrAg$_{0.90}$Al$_{0.35}$Ge$_{0.75}$ and SmAg$_{0.90}$Al$_{0.39}$Ge$_{0.71}$.

PrAg$_{0.90}$Al$_{0.35}$Ge$_{0.75}$			SmAg$_{0.90}$Al$_{0.39}$Ge$_{0.71}$		
Atoms		δ, nm	Atoms		δ, nm
Pr	-1 *M1*	0.3059(7)	Sm	-1 *M1*	0.3031(3)
	-4 *M2*	0.3087(1)		-4 *M2*	0.3043(1)
	-2 *M3*	0.328(1)		-2 *M3*	0.3217(7)
	-4 *M3*	0.3453(1)		-4 *M3*	0.3419(6)
	-4 Pr	0.3742(3)		-4 Sm	0.3675(2)
	-1 *M1*	0.4173(7)		-1 *M1*	0.4087(6)
	-2 Pr	0.44081(8)		-2 Sm	0.43634(5)
M3	-2 *M2*	0.281(1)	*M3*	-2 *M2*	0.2756(5)
	-2 *M1*	0.2810(9)		-2 *M1*	0.2780(2)
	-2 *M3*	0.302(2)		-2 *M3*	0.2984(9)
	-2 Pr	0.328(1)		-2 Sm	0.3217(7)
	-4 Pr	0.3453(1)		-4 Sm	0.3419(6)
M2	-3 *M3*	0.281(1)	*M2*	-3 *M3*	0.2756(5)
	-6 Pr	0.3087(1)		-6 Sm	0.3043(1)
M1	-6 *M3*	0.2810(9)	*M1*	-6 *M3*	0.2780(2)
	-3 Pr	0.3059(7)		-3 Sm	0.3031(3)

M3 = 0.65(3)Ag + 0.35(3)Al   *M3* = 0.61(5)Ag + 0.39(5)Al
M2 = 0.22(8)Ag + 0.78(8)Ge   *M2* = 0.26(7)Ag + 0.74(7)Ge
M1 = 0.32(8)Ag + 0.68(8)Ge   *M1* = 0.36(1)Ag + 0.64(1)Ge

Table 11 Details of the structure refinement for the polycrystalline sample Pr$_{33.3}$Ag$_{26.7}$Al$_{20.0}$Ge$_{20.0}$ (synchrotron data, λ = 0.049063 nm).

Phase		PrAg$_{0.87}$Al$_{0.38}$Ge$_{0.75}$
Space group		$P\bar{6}2m$
Unit-cell parameters	*a*, nm	0.72311(2)
	c, nm	0.44101(2)
	V, nm^3	0.19971(2)
Formula units per cell *Z*		3
Density D_X, g cm^{-3}		7.4682(7)
2θ range, °		4.5-90.0
Number of reflections		1028
FWHM parameters *U, V, W*		0.21994, -0.00725, 0.00032
Asymmetry parameter C_M		-0.00007
Number of refined parameters		27
Reliability factors	R_I	0.0402
	R_p	0.1072
	R_{wp}	0.1211
	R_{dbw}	0.0795

Table 12 Atomic coordinates and isotropic displacement parameters for PrAg$_{0.87}$Al$_{0.38}$Ge$_{0.75}$ (space group $P\bar{6}2m$, *a* = 0.72311(2), *c* = 0.44101(2) nm).

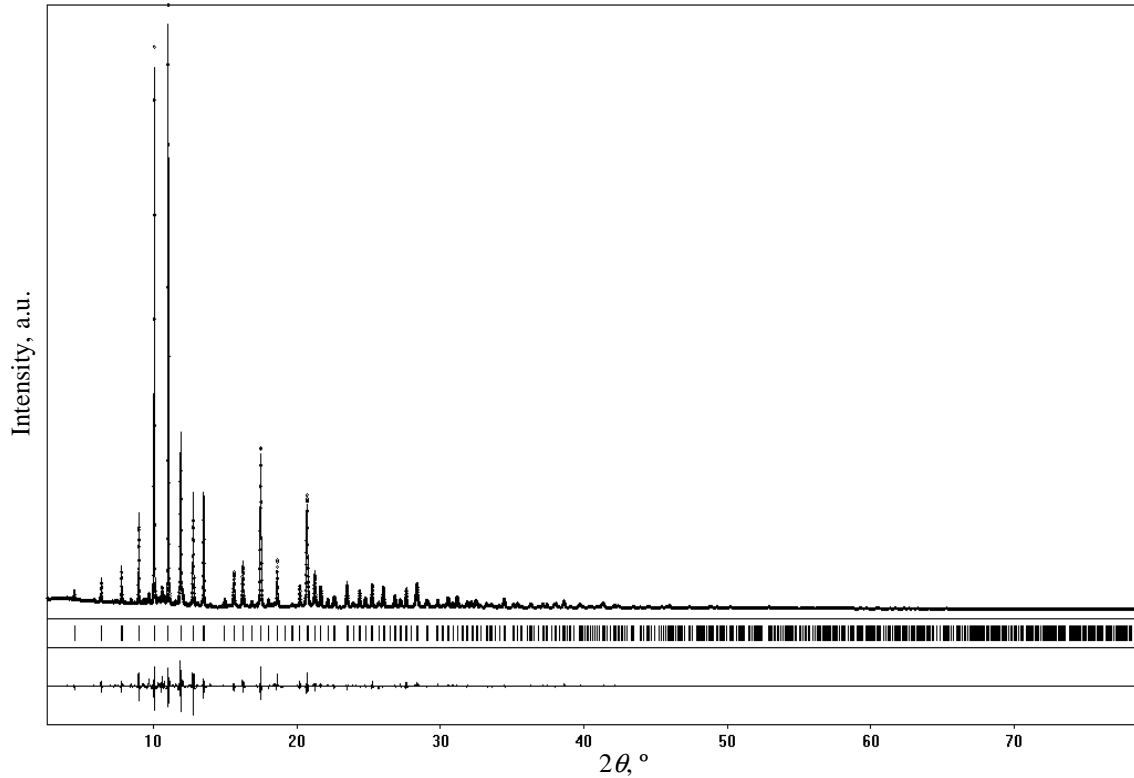| Site	Wyckoff position	*x*	*y*	*z*	B_{iso}, 10^{-2} nm^2	Occupancy
Pr	3*f*	0.57705(9)	0	0	0.57(2)	1
M3	3*g*	0.2402(2)	0	1/2	1.28(5)	0.619(3)Ag + 0.381(3)Al
M2	2*d*	1/3	2/3	1/2	0.81(4)	0.31(1)Ag + 0.69(1)Ge
M1	1*a*	0	0	0	1.17(6)	0.14(1)Ag + 0.86(1)Ge

Fig. 8 Observed (dots), calculated (line) and difference (bottom) X-ray synchrotron diffraction patterns for the Pr$_{33.3}$Ag$_{26.7}$Al$_{20.0}$Ge$_{20.0}$ sample (λ = 0.049063 nm).

Table 13 Anisotropic displacement parameters (10^{-2} nm^2) for PrAg$_{0.87}$Al$_{0.38}$Ge$_{0.75}$.

Site	B_{11}	B_{22}	B_{33}	B_{12}	B_{13}	B_{23}
Pr	0.50(2)	0.44(3)	0.56(2)	1/2B_{22}	0	0
*M*3	1.17(6)	1.10(6)	1.16(6)	1/2B_{22}	0	0
*M*2	0.76(4)	B_{11}	0.66(7)	1/2B_{11}	0	0
*M*1	0.98(7)	B_{11}	1.19(9)	1/2B_{11}	0	0

*M*3 = 0.619(3)Ag + 0.381(3)Al
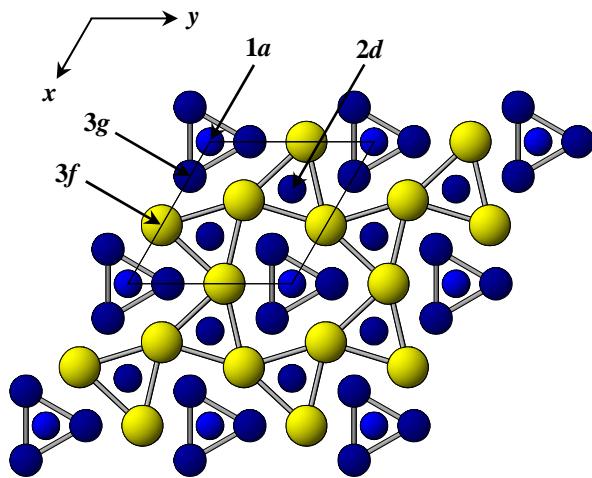*M*2 = 0.31(1)Ag + 0.69(1)Ge
*M*1 = 0.14(1)Ag + 0.86(1)Ge

Fig. 9 Projection of the Fe$_2$P-type structure along [001].

Table 14 Interatomic distances for PrAg$_{0.87}$Al$_{0.38}$Ge$_{0.75}$.

Atoms		δ, nm
Pr	-1 *M*1	0.30584(4)
	-4 *M*2	0.30871(3)
	-2 *M*3	0.32858(7)
	-4 *M*3	0.34527(7)
	-4 Pr	0.37421(5)
	-1 *M*1	0.41727(4)
	-2 Pr	0.44101(2)
*M*3	-2 *M*1	0.28069(5)
	-2 *M*2	0.28085(8)
	-2 *M*3	0.3008(1)
	-2 Pr	0.32858(7)
	-4 Pr	0.34527(7)
*M*2	-3 *M*3	0.28085(8)
	-6 Pr	0.30871(3)
*M*1	-6 *M*3	0.28069(5)
	-3 Pr	0.30584(4)
	-3 Pr	0.41727(4)

*M*3 = 0.619(3)Ag + 0.381(3)Al
*M*2 = 0.31(1)Ag + 0.69(1)Ge
*M*1 = 0.14(1)Ag + 0.86(1)Ge

In the Fe$_2$P-type structure (Fig. 9) columns of trigonal prisms R_6 are joined together by edges to form channels [13]; in these channels columns of trigonal

prisms M_6 are situated. We studied the deformations of the trigonal prisms within the solid solutions with Fe$_2$P-type structure (see Tables 4,5). The height of the trigonal prisms R_6 and M_6 is equal to the *c*-parameter, whereas its base can be calculated by the formulas:

$$a\sqrt{3x_{Pr}^2 - 3x_{Pr} + 1} \text{ (for } R_6\text{) and } \sqrt{3}ax_{M3} \text{ (for } M_6\text{),}$$

where x_{Pr} and x_{M3} are the coordinates of the *R* and *M*3 atoms, respectively. The height/base ratio of the trigonal prisms, which reflects the prism deformations, is greater than 1. It means that the trigonal prisms are stretched along the 6-fold axes. Within the homogeneity range of the Fe$_2$P-type solid solutions the height/base ratio of the trigonal prisms R_6 increases with increasing Al and decreasing Ge (or Ag) content for a fixed Ag (or Ge) content. It should be noted that for the AlB$_2$-type and α-ThSi$_2$-type quaternary solid solutions formed in the {Pr,Sm}–Ag–Al–Ge systems the height/base ratio of the trigonal prisms R_6 is less than 1 (the prisms are compressed) and increases with increasing valence electron concentration per atom of the statistical mixture *M*.

Conclusions

Limited solid solutions based on the ternary compounds PrAg$_{1.40-1.20}$Ge$_{0.60-0.80}$ and SmAg$_{1.40-0.98}$Ge$_{0.60-1.02}$ with the Fe$_2$P-type structure are formed in the quaternary systems *R*–Ag–Al–Ge (*R* = Pr, Sm) at 33.3 at.% *R* and 873 K. Within the homogeneity ranges of the solid solutions the *a*-parameter decreases with increasing Al and decreasing Ge (or Ag) content for a fixed Ag (or Ge) content, whereas the *c*-parameter increases. This is accompanied by an increase (decrease) of the valence electron concentration per atom of the statistical mixture Ag+Al+Ge (VEC$_A$ = 3.55-4.17). A statistical mixture of Ag+Al atoms forms columns of trigonal prisms (3*g* site) with predominantly Ge atoms at the centers (1*a* site), whereas a statistical mixture of Ge+Ag atoms occupy the centers of the trigonal prisms R_6 (2*d* site). The height/base ratio of the trigonal prisms R_6 within the homogeneity range of the Fe$_2$P-type solid solution is greater than 1 and increases with increasing Al and decreasing Ge (or Ag) content for a fixed Ag (or Ge) content.

References

[1] M.M. Dzoba, I.A. Savysyuk, O.O. Shcherban, E.I. Gladyshevskii, *Visn. Lviv. Univ., Ser. Khim.* 36 (1996) 59-65.

[2] I.A. Savysyuk, E.I. Gladyshevskii, R.E. Gladyshevskii, *J. Alloys Compd.* 314 (2001) 167-169.

[3] O.V. Zaplatynsky, P.S. Salamakha, O.L. Sologub, O.S. Procyk, O.I. Bodak, *Pol. J. Chem.* 70 (1996) 267-269.

[4] B. Gibson, R. Pöttgen, R.K. Kremer, A. Simon, K.R.A. Ziebeck, *J. Alloys Compd.* 239 (1996) 34-40.

[5] J.T. Zhao, E. Parthé, *Acta Crystallogr. C* 46 (1990) 2273-2276.

[6] P. Villars, K. Cenzual (Eds.), *Pearson's Crystal Data. Crystal Structure Database for Inorganic Compounds*, ASM International, Materials Park (OH), 2007.

[7] R.A. Young, A.C. Larson, C.O. Paiva-Santos, *Rietveld Analysis of X-Ray and Neutron Powder Diffraction Patterns*, School of Physics, Georgia Institute of Technology, Atlanta, 1998.

[8] L.G. Akselrud, P.Y. Zavalii, Yu.N. Grin, V.K. Pecharsky, B. Baumgartner, E. Wolfel, *Mater. Sci. Forum* 133-136 (1993) 335-340.

[9] R.S. Kozak, R.E. Gladyshevskii, *Ukr. Khim. Zh.* 76(3) (2010) 14-20.

[10] R. Kozak, R. Gladyshevskii, *Coll. Abs. 17 Int. Conf. Solid Compd. Transition Elem.*, Annecy, 2010, p. 68.

[11] R.S. Kozak, R.E. Gladyshevskii, *Phys. Chem. Solid State* 11(4) (2010) 980-990.

[12] E. Parthé, Elements of Inorganic Structural Chemistry, *K. Sutter Parthé Publisher, Petit-Lancy,* 1996, 170 p.

[13] P.I. Krypyakevych, *Structure Types of Intermetallic Compounds*, Nauka, Moscow, 1977, 288 p.